Acta Geodyn. Geomater., Vol. 22, No. 4 (220), 453–464, 2025
DOI: 10.13168/AGG.2025.0032
journal homepage: https://www.irsm.cas.cz/acta

ORIGINAL PAPER

# PROCESSING GRACE LEVEL 2 DATA BASED ON EFFICIENT CALCULATION AND STATISTICAL OPTIONAL SLEPIAN METHOD

**Yu CAO, Nijia QIAN*, Yong FENG, Yueyang HUAN and Yinxiao SUN**

*School of Environment Science and Spatial Informatics, China University of Mining and Technology, Xuzhou 221116, China*

**Corresponding author's e-mail:* nijiaqian@cumt.edu.cn

**ARTICLE INFO**

***Article history:***
Received 8 May 2024
Accepted 12 September 2024
Available online 13 October 2025

***Keywords:***
GRACE
Slepian
Fast
Tikhonov regularization
Power law model
GCV

**ABSTRACT**

The GRACE (Gravity Recovery and Climate Experiment) mission provides critical data for understanding Earth's mass transport, yet its Level 2 products are affected by high-frequency and north-south stripe errors. Traditional Slepian methods, while valuable for regional analysis, face significant computational and storage limitations for high band-limits due to their $L^2 \times L^2$ matrix operations. This study introduces a Fast Statistically Optimal Slepian (FSO-Slepian) method to address these challenges. FSO-Slepian integrates an efficient Slepian function computation (Fast-Slepian), which extends polar cap Slepian techniques to arbitrary regions, with a robust regularization scheme. This regularization employs a generalized Kaula criterion-based prior covariance matrix, Tikhonov regularization, and Generalized Cross-Validation (GCV) for optimal parameter determination, effectively suppressing errors. Experimental results demonstrate that Fast-Slepian significantly accelerates computation (e.g., 3-4 times faster for L=60) while maintaining numerical accuracy comparable to traditional Slepian methods. After regularization, FSO-Slepian effectively removes stripe errors and high-frequency noise, achieving filtering performance comparable to or superior to existing Statistically Optimal Slepian (SO-Slepian) and DDK (Decorrelation and Denoising Kernel) methods in terms of RMSE and uncertainty (e.g., lowest uncertainty of 10.85 cm in the Amazon basin). Time series analysis further confirms its stability and reliability for long-term monitoring, which also highlights the rationality of the application of regularization in the Slepian modeling stage. In conclusion, FSO-Slepian offers an efficient, accurate, and robust solution for GRACE Level 2 data processing, enhancing the practical application of Slepian functions in regional mass change studies and contributing to a more precise understanding of Earth system dynamics.

## 1. INTRODUCTION

GRACE achieves, for the first time in history, time-variable Earth's gravity recovery on a monthly scale (Tapley et al., 2004). The GRACE project has been successfully applied to retrieve the mass transportation within/between different earth systems, including solid earth, cryosphere, ocean, terrestrial water, etc. Due to the interaction between the multiple error sources and the specific mission orbit/formation, there are inevitably errors of different characteristics, in the unconstrained Level 2 products. The most prominent two types are the so called high-frequency errors and the north-south stripe errors (Chambers et al., 2004; Velicogna and Wahr, 2006). Post processing is often necessary to reduce the errors, in order for the products to be applicable in practice.

In 1998, Wahr proposed the Gaussian smoothing function, characterized by Gaussian coefficients that have an inverse relationship with their degree. Additionally, as the filtering radius expands, the signal progressively diminishes (Wahr et al., 1998). In 2006, Sasgen proposed the Wiener filtering to process the spherical harmonic coefficient "series" (Sasgen et al., 2006). Kusche proposed DDK filtering based on the covariance matrix of spherical harmonic coefficients (Kusche, 2007; Kusche et al., 2009). In 2020, a highly parametrized method is proposed: the signal (spherical harmonic coefficients) is parameterized in time domain with a polynomial and seasonal model; the stripe error with a given order and parity is parameterized (in transformed space domain) as a polynomial function of degrees; all the model parameters are estimated simultaneously with weighted least-squares (Crowley and Huang, 2020). In 2022, Yang proposed the low-pass filtering to process the GRACE data (Yang et al., 2022). In 2024, Cao developed a regularization scheme for GRACE data processing based on Slepian named SO-Slepian (Cao et al., 2024). However, Cao used the conventional approach to compute the band-limited Slepian functions for arbitrary regions on the sphere. It requires computing a $L^2 \times L^2$ matrix K and performing its eigen-decomposition, where L denotes the band-limit (in the SH basis). Large band-limit leads to high computational complexity and large storage requirements, thus limiting the better applications of Slepian functions. But for the certain polar cap regions, there is an efficient computational method

**Cite this article as:** Cao Y, Qian N, Feng Y, Huan Y, Sun Y: Processing GRACE Level 2 data based on efficient calculation and statistical optional Slepian method. Acta Geodyn. Geomater., 22, No. 4 (220), 453–464, 2025. DOI: 10.13168/AGG.2025.0032

available for Slepian functions, which helps to keep computational complexity and storage demands manageable (Plattner and Simons, 2015). An efficient algorithm for the approximate computation of Slepian functions for arbitrary regions on the sphere was proposed (Bates et al., 2017), based on the efficient approach for computing Slepian functions over the polar cap region. Compared to the traditional methods, the efficient algorithm which Alice mentioned in 2017 greatly improves the computation speed of the Slepian function, and in the same conditions significantly reduces the storage requirements (Bates et al., 2017). Therefore, this paper adopts the improved method proposed by Alice to process GRACE Level-2 data. This method was used to convert the spherical harmonic basis of GRACE Level-2 to the Slepian basis of the region of interest. Then regularization is applied during the Slepian modeling stage, and a reasonable regularization scheme based on Fast-Slepian for processing GRACE data is derived.

In general, the problems that can be addressed using the Slepian method can be divided into two categories: spatial concentration of finite spectral signals and spectral concentration of finite spatial signals. The GRACE Level 2 data provided by various analysis centers are finite spectral or band-limited. Therefore, when applying the Slepian method to process this data, it addresses the spatial concentration problem of finite spectral signals. The FSO-Slepian method proposed in this paper actually uses the efficient calculation of the Slepian function of the polar cap region on the spherical surface to solve the problems of la large amount of computation, large amount of storage, and time-consuming of the traditional Slepian method. Moreover, a reasonable regularization scheme based on Fast-Slepian is deduced in detail to process GRACE data. This section is the introduction, the second section is the Methodology, and the third section is the Experimental Results and Analysis. The final section is the Conclusion.

## 2. METHOD:

### *2.1. PRINCIPLES OF THE FAST-SLEPIAN METHOD*

Any band-limited signal on a sphere Ω can be expressed as a linear combination of spherical harmonics as shown below (Simons and Dahlen, 2006):

$$\bar{y}(x) = \sum_{l=0}^{L} \sum_{m=-l}^{l} y_{lm} Y_{lm}(x) \quad (1)$$

Here, $\boldsymbol{x}$ represents the location ($\theta_0$, $\phi_0$) of arbitrary point on the sphere Ω, where $\theta_0$ is the colatitude and $\phi_0$ is the longitude. $Y_{lm}$ represents the normalized spherical harmonics, and the $y_{lm}$ represents the spherical harmonic coefficients, where $l$ denotes degree and $m$ denotes order.

Introducing the following defining: R is defined as arbitrary region of the sphere with an area of A, Θ is defined as the smallest spherical cap that encloses the arbitrary interest region R on the sphere with an area of B and the its center point is ($\theta$, $\phi$) $\Theta_0$ is a cap of the polar sphere equal to the area of Θ, with an area of B;

According to (Simons and Dahlen, 2006), it is easy to obtain the Slepian basis function corresponding to $\Theta_0$,$\bar{f}_i(x)$, $1 \le i \le (L+1)^2$. Then the Slepian basis function corresponding to Θ is shown in the following equation:

$$\bar{g}_i(x) = \bar{f}_i\left(\boldsymbol{R}_{\phi-\theta-0}^{T} x\right) \quad (2)$$

The symbol $\boldsymbol{R}_{\phi\text{-}\theta\text{-}0}$ denotes the rotation matrix corresponding to the z-y-z Euler angles $\phi$, $\theta$, and $0$, respectively. Meanwhile, the corresponding $(L+1)^2 \times 1$-dimensional Slepian eigenvector $\boldsymbol{f}_i$ can be easily obtained from (Simons and Dahlen, 2006) for $\Theta_0$, where $1 \le i \le (L+1)^2$. Through a linear transformation, the corresponding $(L+1)^2 \times 1$-dimensional Slepian eigenvector $\boldsymbol{g}_i$ can be easily obtained for Θ, where $g_{ilm}$ denotes the elements of $\boldsymbol{g}_i$. The relationship between the Slepian basis and the spherical harmonic basis is shown as follows.

$$\bar{g}_i(x) = \sum_{l=0}^{L} \sum_{m=-l}^{l} g_{ilm} Y_{lm}(x) \quad (3)$$

Represent the signals in (1) as a linear combination of Slepian bases.

$$\bar{y}(x) = \sum_{i=1}^{(L+1)^2} \beta_i \bar{g}_i(x) \quad (4)$$

where the $\beta_i$ is the Slepian coefficient.

Figure 1 shows the 3721 energy concentrations (means eigenvalues λ) and the corresponding sum of the first energy concentrations as a ratio of the total energy, obtained for the 60 th-degree Slepian basis functions in the polar cap radius of Θ= π/6. From Figure 1, it can be observed that the concentration of energy for Slepian basis functions becomes closer to 1 as they appear earlier. As the index ' $i$ ' becomes sufficiently large, the corresponding $\lambda_i$ becomes smaller, and as a result, the energy of $\bar{f}_i(x)$ becomes small enough to be negligible. Based on this, it is possible to truncate the right side of equation (4) to obtain a simpler model with fewer unknowns. For instance, equation (5) computes the Shannon number N, which only includes a finite number of significant non-zero feature signals.

$$N = (L+1)^2 \frac{\int_R d\sigma}{\int_\Omega d\sigma} = (L+1)^2 \frac{B}{4\pi} \quad (5)$$

Therefore, equation (4) is approximated as follows:

$$\bar{y}(x) = \sum_{i=1}^{(L+1)^2} \beta_i \bar{g}_i(x) \approx \sum_{i=1}^{N} \beta_i \bar{g}_i(x) \quad (6)$$

For a signal in Θ of the form $\bar{z}(x) = \sum_{i=1}^{N} z_i \bar{g}_i(x)$, choose the appropriate $z_i$ to maximize the following expression (Bates et al., 2017):

$$\frac{\int_R [\bar{z}(x)]^2 d\sigma(x)}{\int_\Theta [\bar{z}(x)]^2 d\sigma(x)} = \frac{\sum_{i=1}^{N} \sum_{i=1}^{N} z_i z_j k_{ij}}{\sum_{i=1}^{N} z_i^2} max \quad (7)$$

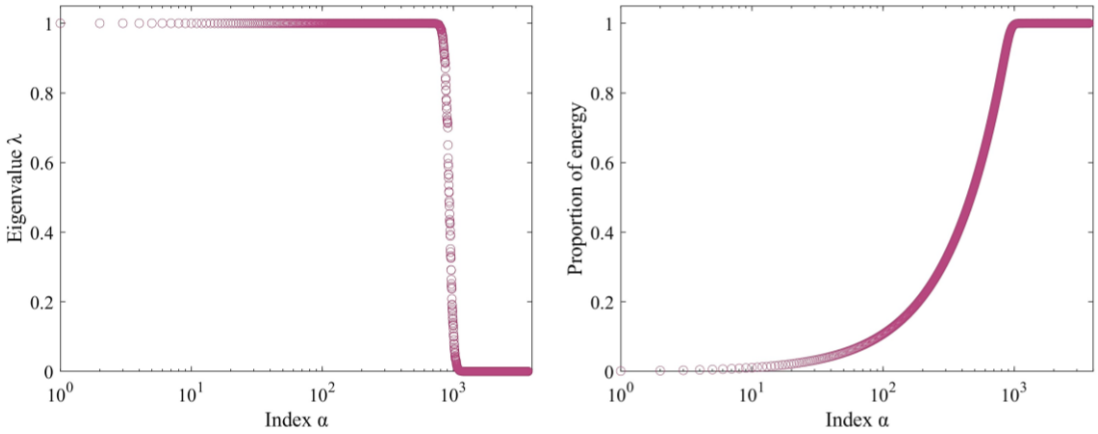


**Fig. 1** The Eigenvalue λ corresponding to the 3721 Slepian basis function expanded up to degree-60 (left) and the corresponding ratio of the sum of the energy concentration of the first a items to the total energy (right), (polar cap radius of Θ= π/6 as an example).

Here $k_{ij}$ is shown as follows:

$$k_{ij} = \int_R \left[\sum_{i=1}^{N}\sum_{i=1}^{N} \bar{g}_i(x)\bar{g}_j(x)\right] d\sigma(x) \quad (8)$$

According to (5), it can be known that the vector $\boldsymbol{h}$ composed of $z_i$ satisfies the eigenequation shown below:

$$\boldsymbol{Kh} = \boldsymbol{\lambda h} \quad (9)$$

Represent the eigenvectors corresponding to the above equation as $\boldsymbol{h}_i$, and introduce a new basis as shown in the following equation:

$$\bar{h}_j(x) = \sum_{i=1}^{N} h_{ji}\bar{g}_j(x) \quad (10)$$

Any signal in R can be represented as a linear combination of new bases as shown in the following equation:

$$\bar{y}(x) = \sum_{j=1}^{N} \alpha_j \bar{h}_j(x) \quad (11)$$

Combining (9) and (3), we can get the following equation:

$$\begin{aligned}\bar{y}(x) &= \sum_{l=0}^{L}\sum_{m=-l}^{l} y_{lm}Y_{lm}(x) \approx \sum_{j=1}^{N} \alpha_j \bar{h}_j(x)\,, \\ &= \sum_{j=1}^{N}\sum_{i=1}^{N} \alpha_j h_{ji}\bar{g}_i(x) \\ &= \sum_{j=1}^{N}\sum_{i=1}^{N}\sum_{l=0}^{L}\sum_{m=-l}^{l} \alpha_j h_{ji} g_{ilm} Y_{lm}(x) \end{aligned} \quad (12)$$

Define $a_{jlm} = \sum_{i=1}^{N} h_{ji} g_{ilm}$, so the above equation is equivalent to the following expression:

$$\bar{y}(x) = \sum_{j=1}^{N}\sum_{l=0}^{L}\sum_{m=-l}^{l} \alpha_j a_{jlm} Y_{lm}(x) \quad (13)$$

Considering the arbitrariness of the position $\boldsymbol{x}$, by combining formula (1), the following equation can be obtained:

$$y_{lm} = \sum_{j=1}^{N}\left[\alpha_j a_{jlm}\right] \quad (14)$$

Written in vector-matrix form, it is as follows:

$$\boldsymbol{y} = \boldsymbol{A\alpha} \quad (15)$$

The parameter estimation is shown as follows:

$$\hat{\boldsymbol{\alpha}} = A^{-1}\boldsymbol{y} \quad (16)$$

However, without considering the statistical information of the observation $\boldsymbol{y}$ in equation (14), (its covariance matrix $\boldsymbol{Q}$), the statistical information of measurement errors (including striping error and high-frequency noise) can't be reflected, and the effect of stripe removal can't be achieved (Cao et al., 2024). Therefore, we should consider the covariance matrix $\boldsymbol{Q}$ to remove the effect of stripe.

In the next section the optimal estimation of the parameter $\boldsymbol{a}$ will be elaborated in detail.

### *2.2. OPTIMAL ESTIMATION OF PARAMETER a*

According the well-known power law model (generalized Kaula criterion) (Cao et al., 2024; Sasgen et al., 2006), this paper constructs the prior covariance matrix of parameters and uses it as the Tikhonov regularization matrix. According to the generalized Kaula criterion, a suitable prior variance for $y_{lm}$ is chosen as shown below.

$$var[y_{lm}] = l^{-\mu} \quad (17)$$

The $\mu$ is a hyperparameter that needs to be adjusted. The prior covariance matrix $\boldsymbol{S}$ of vector $y$ is a diagonal matrix with the above variances as diagonal elements. Therefore, the prior covariance matrix of parameter $a$ is defined as $\boldsymbol{P}$ ($\boldsymbol{P} = cov[\boldsymbol{\alpha}] = cov[\boldsymbol{A}^T y] = \boldsymbol{A}^T\boldsymbol{S}\boldsymbol{A}$).

Then the definition and calculation formula of the Tikhonov regularization estimation with formula (13) as the observation equation is as follows,

$$\begin{aligned}\hat{\boldsymbol{\alpha}} &= \underset{\alpha}{argmin}[(\boldsymbol{y} - \boldsymbol{A}\alpha)^T\boldsymbol{Q}^{-1}(y - \boldsymbol{A}\alpha) + \sigma\alpha^T\boldsymbol{P}^{-1}\alpha] \\ &= (\boldsymbol{A}^T\boldsymbol{Q}^{-1}\boldsymbol{A} + \sigma\boldsymbol{P}^{-1})^{-1}\boldsymbol{A}^T\boldsymbol{Q}^{-1}y \end{aligned} \quad (18)$$

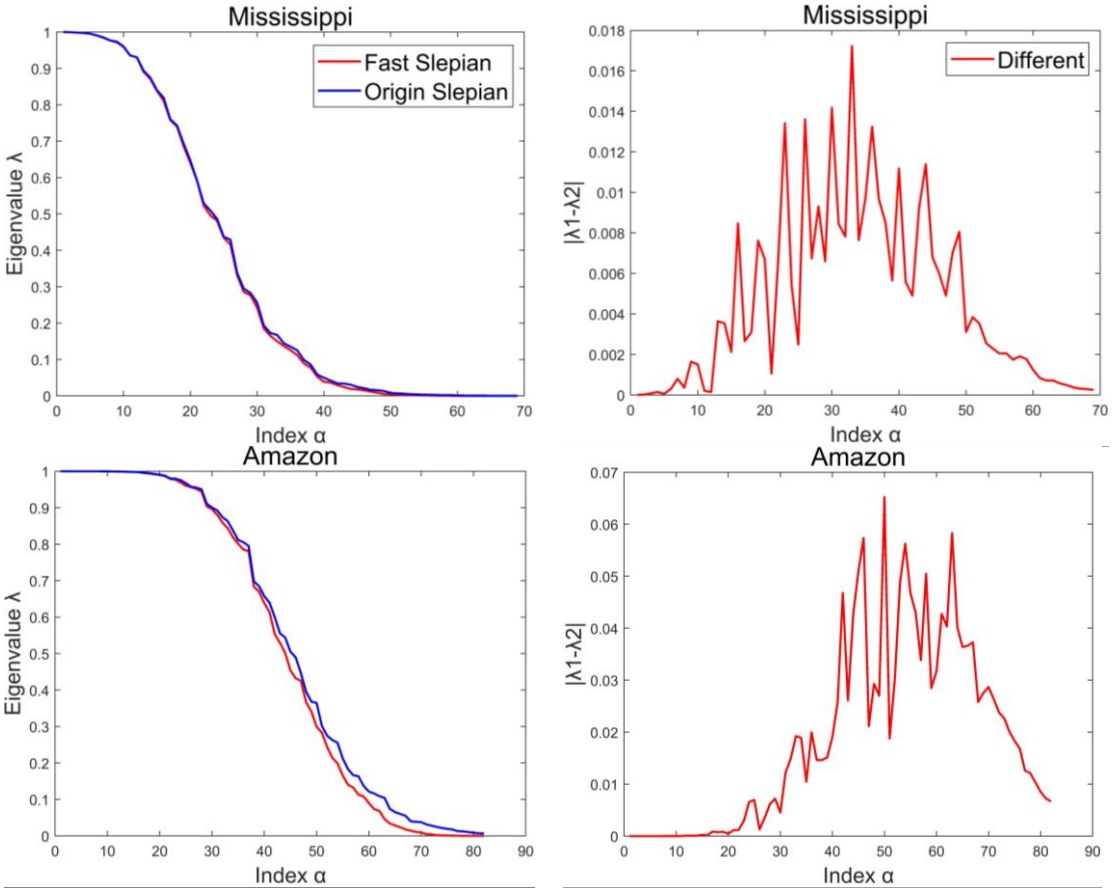


**Fig. 2** The eigenvalues λ (left) of the 60th-degree Mississippi and Amazon calculated using Fast Slepian and the Origin Slepian, as well as the absolute value of the difference between the two methods |λ1-λ2| (Right) (Truncated to NΘ, ΘMississippi=69, ΘAmazon=82).

The $\sigma$ is also a hyperparameter that needs to be adjusted. The commonly used criteria for determining the regularization parameter are the L-curve method (Hansen and O'Leary, 1993), Generalized Cross-Validation (GCV) (Golub et al., 1979; Qian et al., 2021), and minimum Mean Squared Error (MSE) criteria (Hoerl and Kennard, 2000; Ji et al., 2022; Shen et al., 2012). Each of these criteria has its own merits and limitations (Xu, 1992). In this work we choose the GCV.

$$GCV = \frac{(\boldsymbol{y}-\boldsymbol{A}\hat{\alpha})^T\boldsymbol{Q}^{-1}(y-\boldsymbol{A}\hat{\alpha})}{((L+1)^2-\mathrm{tr}[\boldsymbol{A}(\boldsymbol{A}^T\boldsymbol{Q}^{-1}\boldsymbol{A}+\sigma\boldsymbol{P}^{-1})^{-1}\boldsymbol{A}^T\boldsymbol{Q}^{-1}])^2} \quad (19)$$

The selection of the two hyperparameters $\mu$ and $\sigma$ in the formulas (15) and (16) is performed based on the Generalized Cross-Validation (GCV) method as shown in equation (17). In this paper we call it Fast Statistically Optimal Slepian (FSO-Slepian).

## 3. EXPERIMENTAL RESULTS AND ANALYSIS

### 3.1. *FAST SLEPIAN ANALYSIS*

This section aims to evaluate the numerical accuracy of the Slepian functions and eigenvalues obtained through the proposed Fast Slepian method across various regions of the sphere. We will also assess the computational complexity and storage requirements of the method. Specifically, we analyze two major river basins: the Amazon and Mississippi. The left side of Figure 2 shows the eigenvalue spectra of Mississippi and Amazon obtained using the Origin $\lambda_\alpha(\alpha=1,2,\ldots,N_\Theta)$ and fast method $\lambda_\alpha(\alpha=1,2,\ldots,N_\Theta)$. And the absolute difference in the eigenvalues computed using the origin method and the fast method $|\lambda_1-\lambda_2|$ is plotted in the right side of Figure 2**.** From Figure 2, we observe that the eigenvalues obtained from both methods are comparable, with the differences between the eigenvalues from the original method and the Fast Slepian method being on the order of $10^{-2}$ or less. This indicates a high level of agreement between the two methods.

Due to the smooth spreading from the center, Slepian basis functions located near the boundary and far away from the center of the integration area exhibit

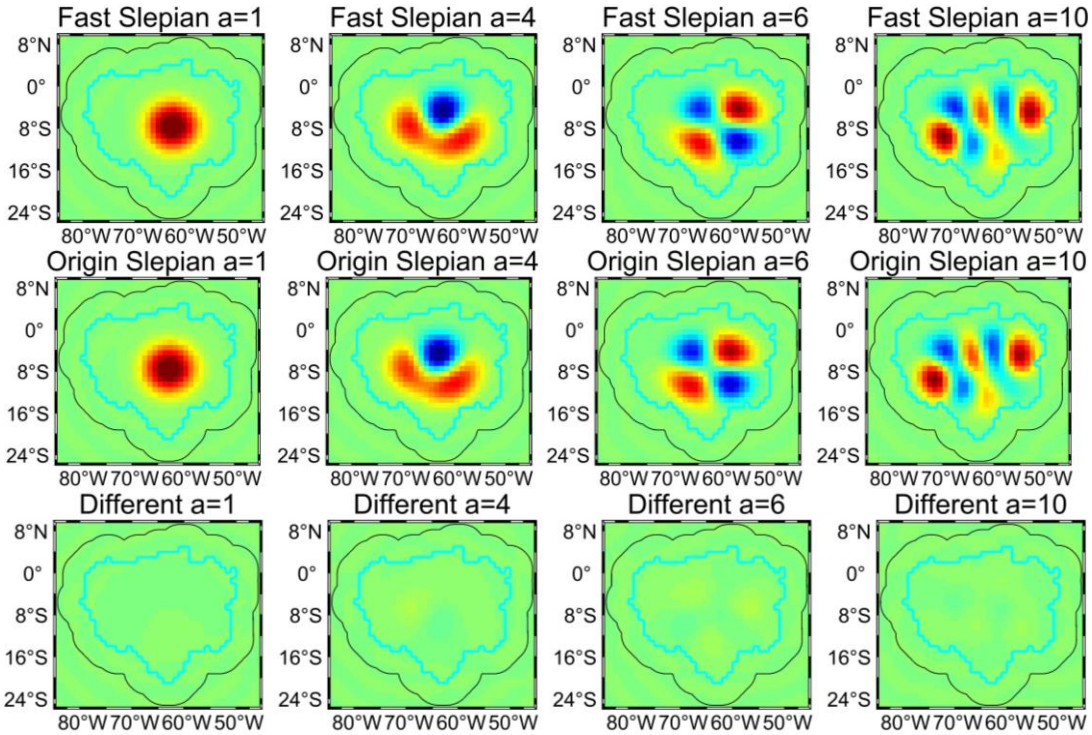


**Fig. 3** Signal distribution of the 1st, 4th, 6th and 10th Slepian basis functions computed using Fast Slepian and the Origin Slepian and the difference between the two methods (Amazon as an example), the inner blue contour is the boundary of Amazon and the outer black contour is the extended boundary for integral calculation

**Table 1** Calculation time of the band-constrained Slepian function at L =60 for Mississippi, Yangtze and Amazon (unit: seconds).

| Region \ Method | Fast Slepian | Origin Slepian |
|---|---|---|
| Mississippi | 208.03 | 812.53 |
| Yangtze | 198.36 | 762.41 |
| Amazon | 216.93 | 700.82 |

a reduced sensitivity (Cheng et al., 2021; Harig and Simons, 2012). Therefore, in order to concentrate the signal in the target region as much as possible in the study area, a buffer zone analysis was performed on the study area to establish an appropriately sized buffer zone. In this paper, the buffer selection for the test area is three degrees. Figure 3 shows the signal distributions of the 1st, 4th, 6th and 10th Slepian basis functions calculated using Fast Slepian and the Origin Slepian method, as well as the differences between these two methods. From the third line, which is the difference between the two methods, we can clearly see that only minor differences remain in the regions, further indicating the high consistency between the two methods.

Table 1 shows the time taken to calculate the Slepian functions with band-limit L=60 for Amazon and Mississippi. All methods were implemented using MATLAB2018b on a laptop computer equipped with a 2.3GHz Intel Core i5-8300 processor and 16GB of RAM.

From Table 1, it is clear that the fast Slepian is several times faster than the Origin Slepian calculation.

### *3.2. ANALYSIS OF FILTERING EFFECT*

The data used in this paper were provided by the Center for Space Research (CSR), University of Texas Austin, 136 months from April 2002 to June 2014 with GRACE Level-2 RL05 (Release-05) spherical harmonic coefficients up to degree 60 (Missing months are not considered). The spherical harmonic coefficients and their corresponding covariance matrix used in the experiments of this paper can be downloaded from the website: http://download.csr.utexas.edu/outgoing/grace/.

Before conducting the experiments, the following pre-processing steps are applied to the spherical harmonic coefficients:

1. The first four terms of the spherical harmonic coefficients are omitted.
2. The mean value of the coefficients during the period from 2004 to 2009 is subtracted.
3. The coefficients are adjusted for glacier isostatic adjustment (GIA) using the ICE-6G_D model.

The arbitrariness of variable x in equation (1) allows for the arbitrary selection of experimental regions. Therefore, in this paper we choose the

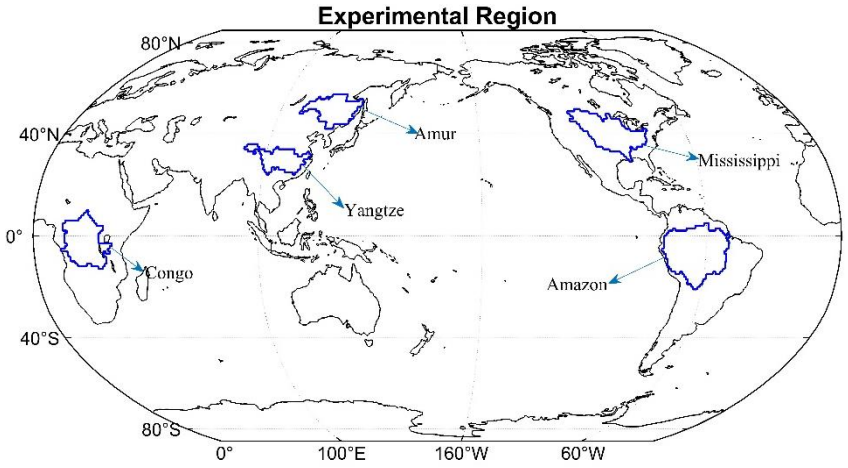


**Fig. 4** Experimental region.

Amazon, Amur, Congo, Mississippi, and Yangtze to verify the effectiveness of the method mentioned in this paper. Figure 4 shows the selected regions

Changes in quality are usually represented by Equivalent Water Height (EWH), and the following equation can be used to obtain changes in EWH on a global scale.

$$\Delta H = \frac{ap_{ave}}{3\rho_w}\sum_{l=0}^{L}\sum_{m=o}^{l}\frac{2l+1}{1+kl}\bar{P}_{lm}(cos\,\theta)(\Delta C_{lm}\,cos(m\lambda) + +\Delta S_{lm}\,sin(m\lambda)) \quad (20)$$

In the equation, $\Delta H$ is the change in Equivalent Water Height, $a$ is the radius of the Earth, $\rho_{ave}$ is the average density of the Earth, $\rho_w$ is the density of water,

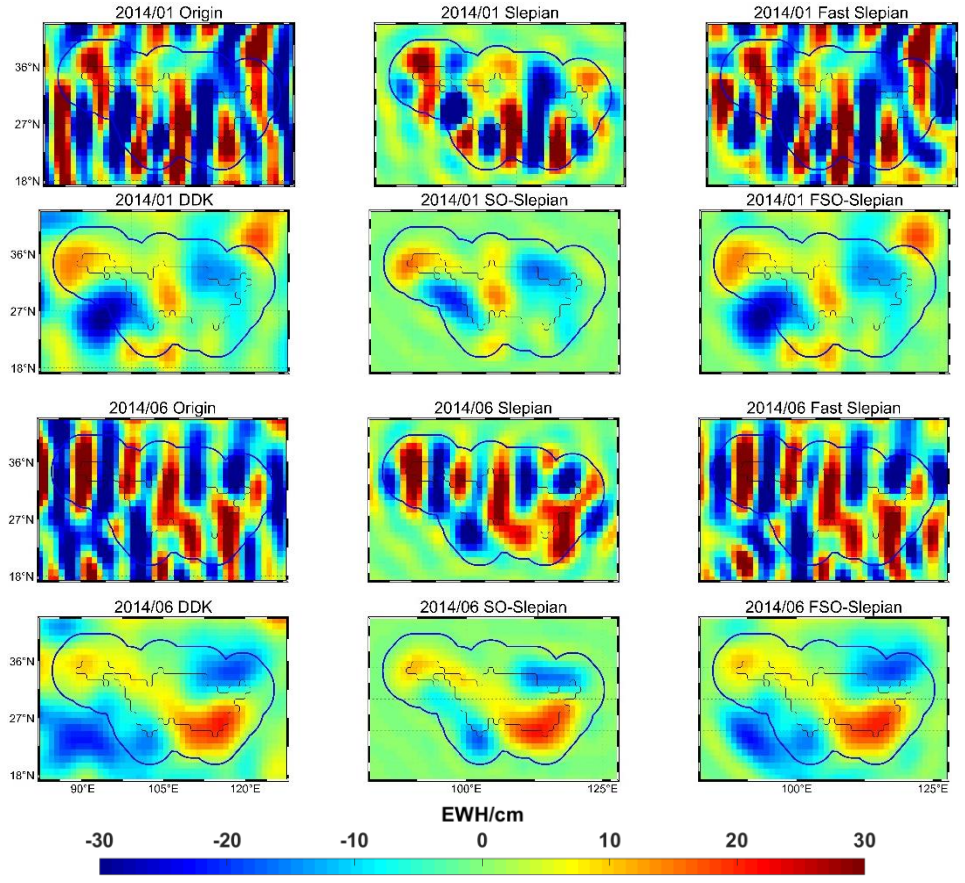


**Fig. 5** The processed CSR data results of the Yangtze in January and June 2014 using Slepian, Fast- Slepian, SO-Slepian, FSO-Slepian and DDK methods, as well as the corresponding original results (the inner black contour is the boundary of Amazon and the outer blue contour is the extended boundary for integral calculation.

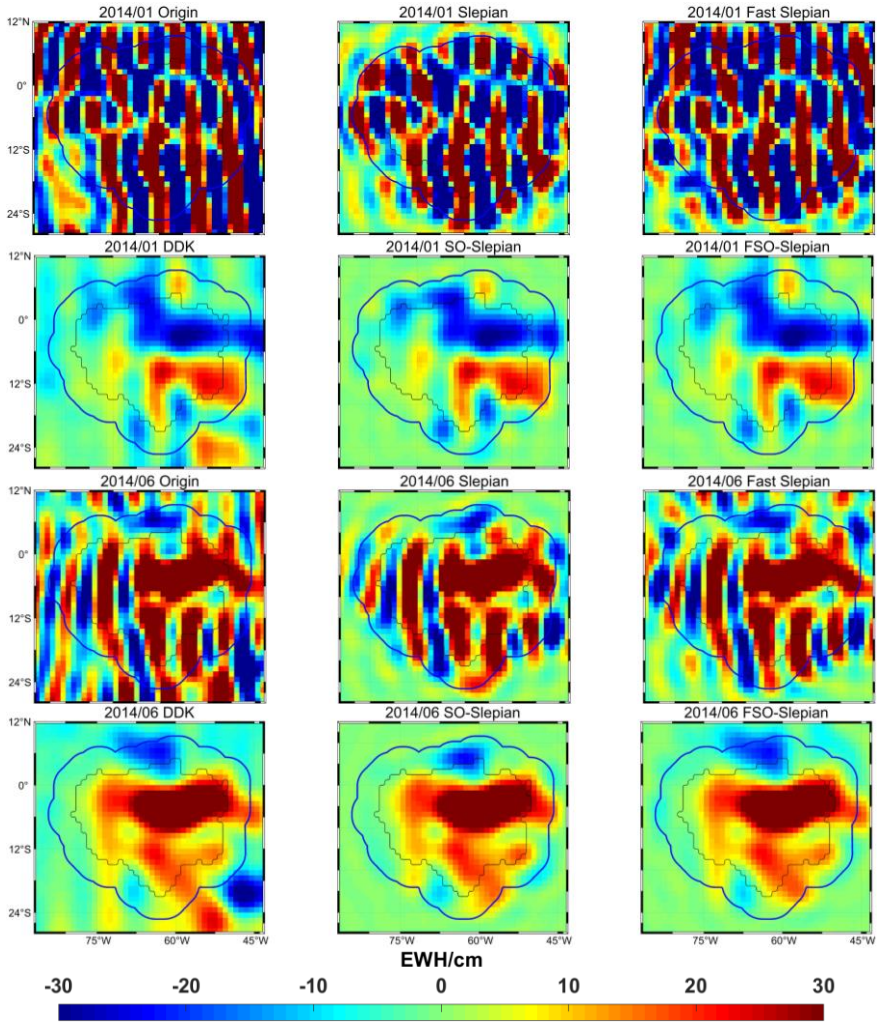


**Fig. 6** The processed CSR data results of the Amazon in January and June 2014 using Slepian, Fast- Slepian, SO-Slepian, FSO-Slepian and DDK methods, as well as the corresponding original results (the inner black contour is the boundary of Amazon and the outer blue contour is the extended boundary for integral calculation).

$k_l$ is the load Love number, and $\theta$ and $\lambda$ is the geocentric latitude and longitude, respectively. Therefore, the change in Equivalent Water Height in the region R can be obtained as follows:

$$\Delta H_{region} = \frac{ap_{ave}}{3\rho_w} \sum_{l=0}^{L} \sum_{m=-l}^{l} \frac{2l+1}{1+kl} \sum_{i=1}^{N} \hat{\alpha}_i a_{ilm} Y_{lm}(x) \tag{21}$$

From Cao, we can get the similarity between the DDK filtering method and SO-Slepian proposed in Cao (2024), the same parameters are often used for comparison analysis (Cao et al., 2024). Therefore Figure 5 and Figure 6 show the EWH grid plots of unconstrained solutions, Slepian (refers to traditional origin Slepian), Fast Slepian, DDK, SO-Slepian, FSO-Slepian in the Yangtze and Amazon for January and June 2014.

From the above Figure 5 and Figure 6, we can clearly see that neither the traditional Slepian nor the Fast Slepian can remove the band error, and the result is only the display of the gravity signal in different coordinates, which needs to be regularized to remove the band error. After regularization it can be known that FSO-Slepian and SO-Slepian have almost the same filtering effect compared with DDK. Figure 7 shows the EWH differences of the Yangtze and Amazon between the two Slepian methods before and after regularization in January and June 2014. From Figure 7, we can clearly see that Fast-Slepian and Origin-Slepian have almost the same effect on the reserved region signals, and some of the remaining signals in the region are due to the error caused by the truncation of the basis function. For the filtered results, the bands in the region are basically completely removed, and the filtered results of the two methods show almost the same effect in the region.

In order to further describe the specific accuracy of the spherical harmonic coefficients of each degree, the accuracy of the gravitational field model can be represented by the sum of the squares of the geoid errors of each degree (Feng et al., 2024; Luthcke et al., 2006).

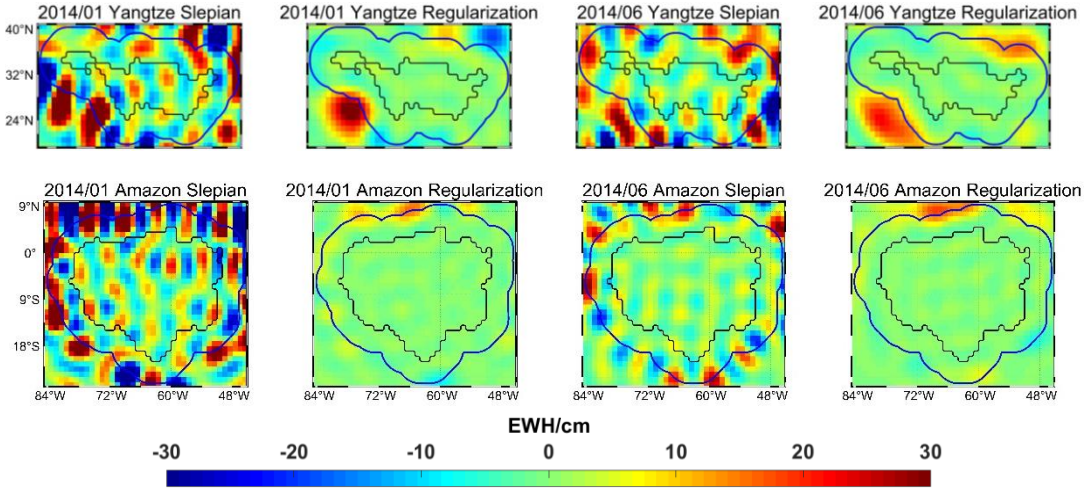


**Fig. 7** The difference of region EWH between Fast Slepian and Origin Slepian (The first and third columns) and FSO -Slepian and SO-Slepian (The second and fourth columns) (the inner black contour is the boundary of Amazon and the outer blue contour is the extended boundary for integral calculation).

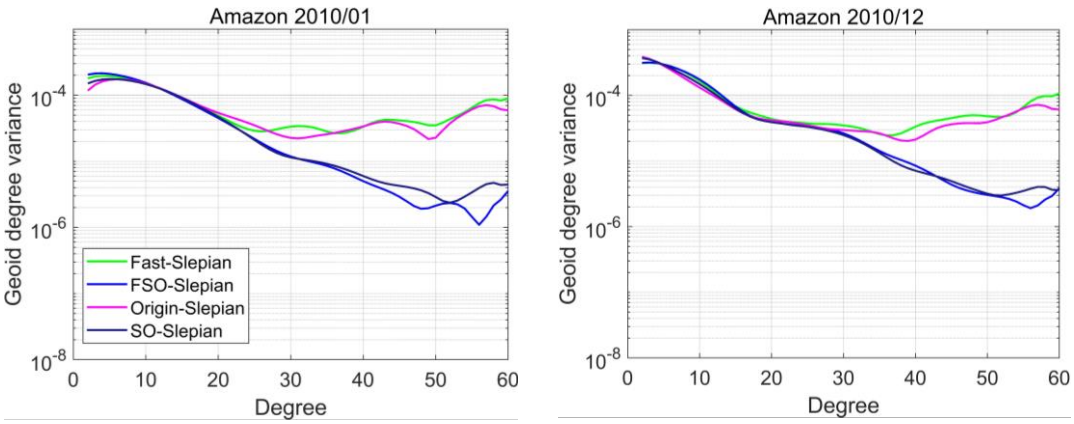


**Fig. 8** January and December 2010 the solutions of Origin-Slepian, Fast- Slepian, SO-Slepian and FSO-Slepian of the geoid degree error.

$$\delta N_l = a\sqrt{\sum_{m=0}^{l}(\delta C_{lm}^2 + \delta S_{lm}^2)} \tag{22}$$

where $\delta \boldsymbol{C}_{lm}$ and $\delta \boldsymbol{S}_{lm}$ denote the error of the spherical harmonic coefficient, $\delta \boldsymbol{N}_l$ is the error corresponding to the spherical harmonic coefficient of each degree, and $\boldsymbol{a}$ is the radius of the earth. Figure 8 takes the geoid degree variance for January and December 2010 as an example.

It is generally considered that the low-degree term ($l$ < 20) is a reflection of the time-varying signal of the gravitational field, while the high- degree term ($l$ > 30) is mainly the noise information of the GRACE/GFO data, and the mixture of signal and noise is between the two (20 < $l$ <30) (Chen et al., 2016; Qian et al., 2022). From Figure 8, it can be clearly concluded that the ability of these four methods to retain signals in the 0-20th degree is almost the same, and the corresponding geoid degree variance before and after regularization is very similar in the 20-30th degree transition stage, which further indicates that the Fast-Slepian proposed in this paper has almost the same effect as the traditional Slepian.

In order to further quantitatively evaluate the performance of the FSO-Slepian method, the calculation formula of RMSE was introduced.

$$RMSE_i = \sqrt{\sum_{x=1}^{m}\sum_{y=1}^{n}\frac{[grido_i(y,x) - gridm_i(y,x)]^2}{m \cdot n}} \tag{23}$$

where *grido* is the regional EWH grid dot value of the spherical harmonic coefficient unconstrained solution and the constrained solution, *girdm* is the regional EWH grid dot value of the CSR-mascon solution, $x$ and $y$ are the indexes of the longitude and latitude direction regional grid points, $i$ is time. Table 2 lists the RMSE of the six methods involved in this paper for the five regions.

Combined with Table 2, Figure 5 and Figure 6, we can clearly see that the Slepain method after

**Table 2** RMSE of the six methods.

| | Origin | Slepain | Fast-Slepian | SO-Slepian | FSO-Slepian | DDK |
|---|---|---|---|---|---|---|
| Amazon | 40.489 | 35.844 | 39.157 | 7.431 | 7.439 | 7.225 |
| Mississippi | 31.836 | 26.551 | 31.109 | 5.855 | 5.921 | 6.264 |
| Yangtze | 36.726 | 31.856 | 36.247 | 9.353 | 6.768 | 6.750 |
| Amur | 24.047 | 21.759 | 23.859 | 4.534 | 4.444 | 4.408 |
| Congo | 39.369 | 33.112 | 37.763 | 6.592 | 6.010 | 5.160 |

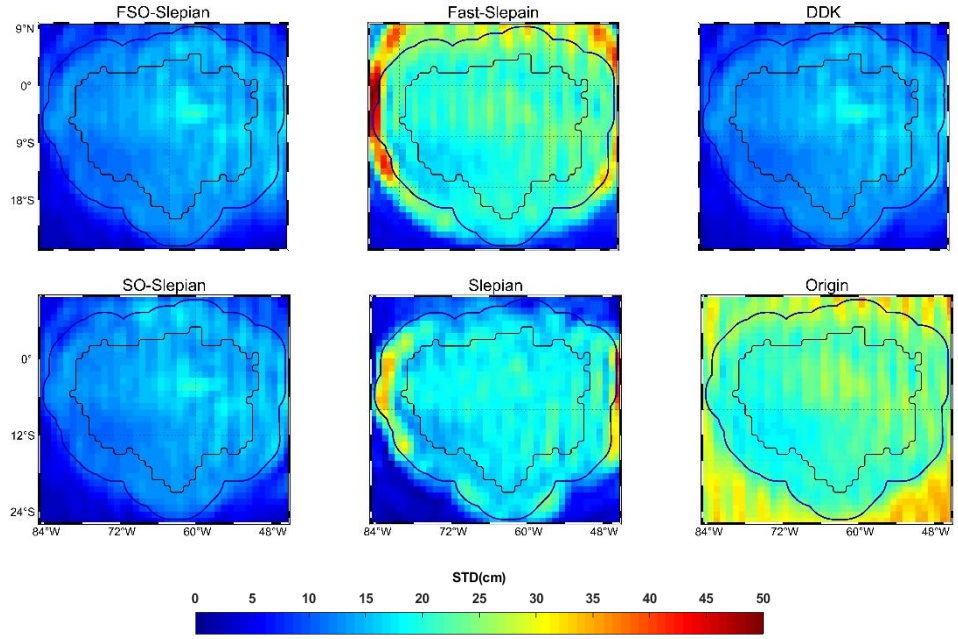


**Fig. 9** Taking the Amazon as an example, the uncertainty grid diagram of six methods FSO-Slepian, SO-Slepian, DDK, Slepain, and Origin (CSR mascon data is used as a reference).

regularization can effectively reduce the impact of stripe error. Even though the RSME of FSO-Slepian is not the smallest in the region, the difference with DDK and SO-Slepian is very weak. It is sufficient to illustrate the effectiveness of FSO-Slepian and the rationality of the Fast-Slepian-based regularization scheme derived in this paper.

In 2021 Chen pointed out that the three-cornered hat (TCH) method provides a technique for assessing the approximate uncertainty of the GRACE/GFO mass field when the true signal is not known (Chen et al., 2021). Therefore, in order to more objectively describe the uncertainty of the change of the earth's mass estimated by FSO-Slepian, the TCH method can verify the performance of the FSO-Slepian method. The toolkit for implementing TCH can be found here.

(https://www.hydroshare.org/resource/63c8cd8f63ec49ebabdca45826219a60/

For specific calculation formulas, please refer to Appendix I.

Figure 9 shows the TCH method was used to estimate six methods (FSO-Slepian, SO-Slepian, DDK, Slepain, Fast-Slepian and Origin) and plot the uncertainty grid of the study area in the form of standard deviation (STD).

Taking the CSR-mascon solution as the reference, the uncertainty of the above processing methods is as follows (FSO-Slepian: 10.85 cm; Fast-Slepain: 20.18 cm; DDK: 10.93 cm; SO-Slepian: 10.99 cm; Slepain: 14.66 cm; Origin: 25.11 cm). Combined with the uncertain grid diagram of Figure 9, it can be clearly seen t hat the regional uncertainty of DDK, FSO-Slepian and SO-Slepian is very similar, and the minimum FSO-Slepian proposd in this paper is 10.85 cm.

### *3.3. TIME SERIES ANALYSIS*

This paper uses a total of 136 months of GRACE spherical harmonic coefficients from April 2002 to June 2014 (including missing months) to obtain region EWH through different filtering methods, including Origin-Slepian, SO-Slepian, Fast-Slepian and FSO-Slepian. Figure 10 shows the EWH time series obtained by Origin-Slepian, Fast- Slepian, SO-Slepian and FSO-Slepian methods in the five selected regions (left), as well as the differences (right) (missing months are ignored in the plot). From the EWH time series (left column), both before and after regularization corresponding time series are very similar and it basically coincides. From the differences (right column), the regularized difference is basically around 0. It further indicates that the Fast-Slepian mentioned in this paper has almost the same effect as the traditional Slepian.

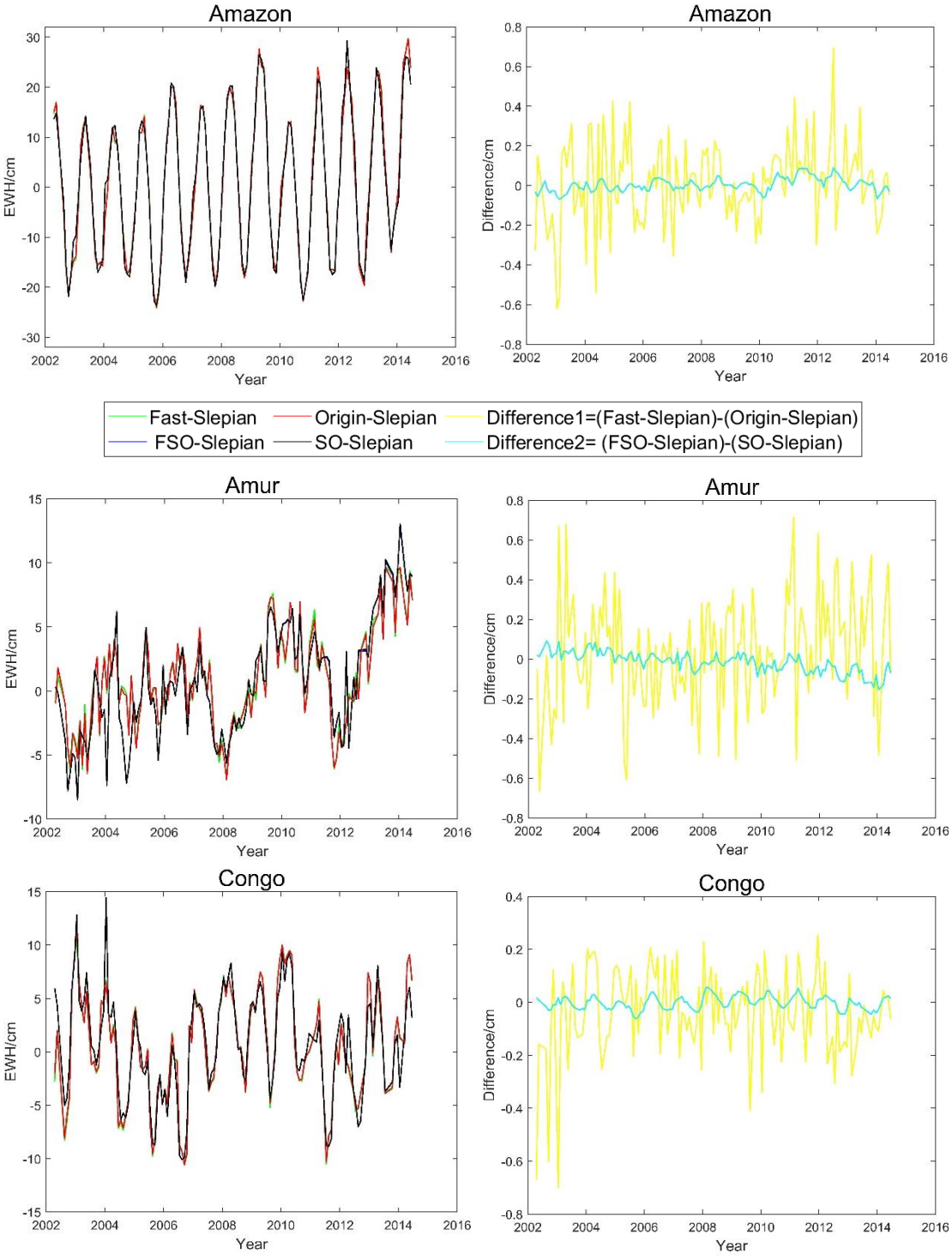


**Fig. 10** Changes in EWH over time in five regions filtered by Origin-Slepian, Fast- Slepian , SO-Slepian and FSO-Slepian (left) and differences (right).

Figure 11 illustrates the root mean square (RMS) of the grid in the Yangtze and Amazon. In terms of error level, both FSO-Slepian and SO-Slepian exhibit close values and minimal errors. Combining the above information with the results shown in Figure 9 and Table 2, it can be concluded that the Fast-Slepian mentioned in this paper has almost the same effect as the traditional Slepian both before and after regularization.

## 4. CONCLUSION

This paper applies the Fast-Slepian function with regularization to the GRACE Level-2 data. The data used in this study are the CSR RL05 GRACE Level-2 products from April 2002 to June 2014. The regional mass changes are obtained by applying constraints and compared with the traditional Slepian both before and after regularization. The following results are obtained.

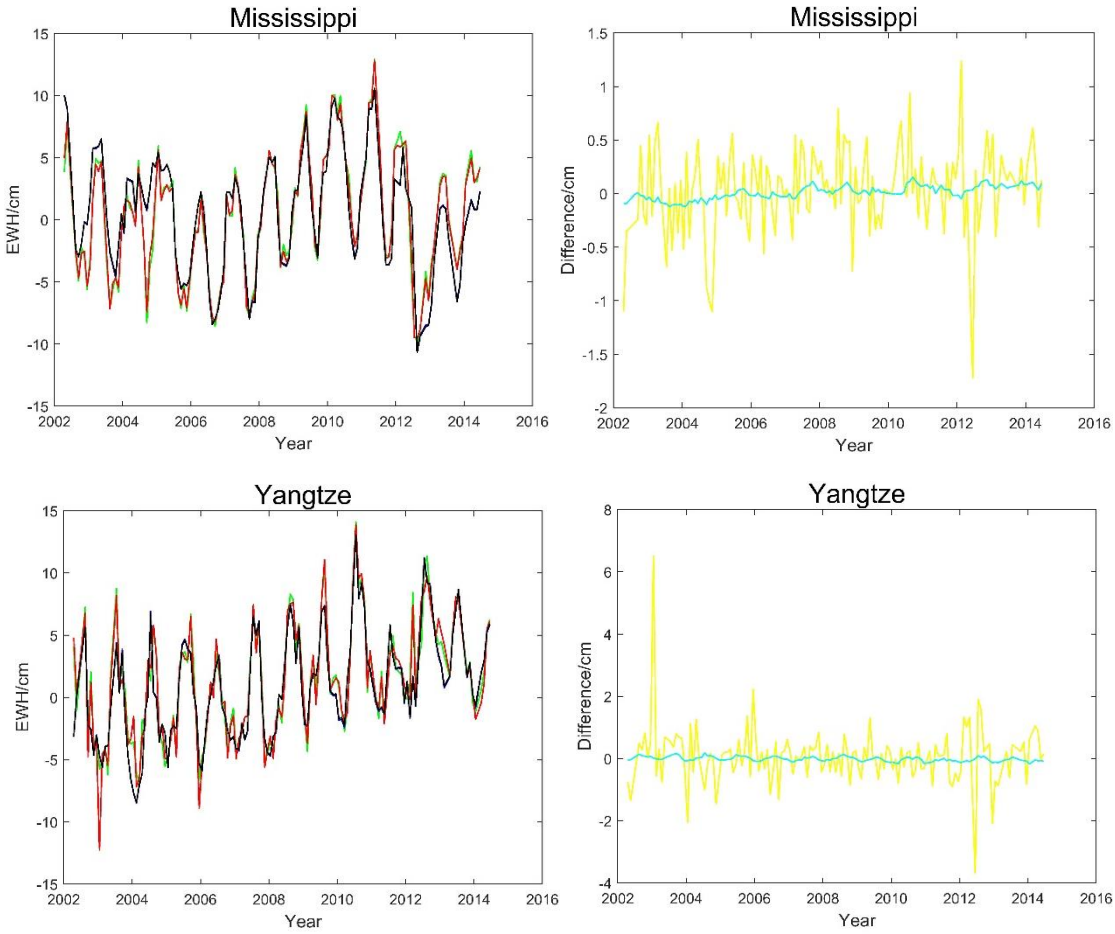


**Fig. 10** Continued.

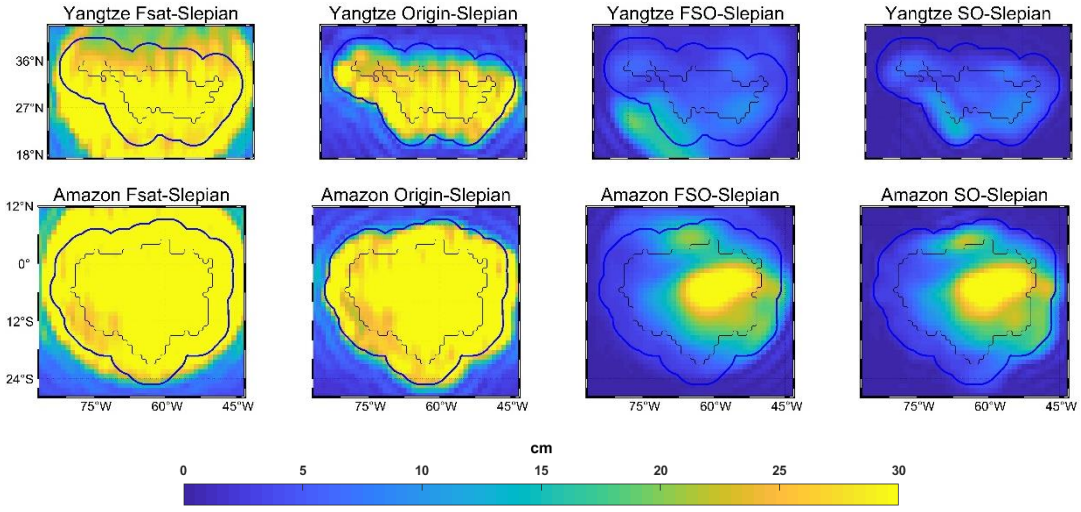


**Fig. 11** RMS of EWH for Origin-Slepian, Fast- Slepian, SO-Slepian and FSO-Slepian filtering methods in the Yangtze and Amazon, April 2002 to June 2014.

1. From the running time and the calculated Slepian basis function, it can be concluded that Fast-Slepian and Origin-Slepian not only have nearly the same effect, but also the Fast-Slepian have much faster computation speed than Origin-Slepian.
2. From the regional grid and time series, it can be known that FSO-Slepian and SO-Slepian have almost the same filtering effect, which also highlights the rationality of the application of regularization in the Slepian modeling stage in this study.

**FUNDING**

This research was funded by the National Natural Science Foundation of China (Grant No. 42504028); the Basic Research Program of Jiangsu Province (Grant No. BK20241665); the Fundamental Research Funds for the Central Universities (Grant No. 2025QN1109)

**CONFLICT OF INTEREST**

The authors declare that the research was conducted in the absence of any commercial or financial relationships that could be construed as a potential conflict of interest.

**REFERENCES**

Bates, A.P., Khalid, Z. and Kennedy, R.A.: 2017, Efficient computation of Slepian functions for arbitrary regions on the sphere. IEEE Trans. Signal Process., 65, 4379–4393. DOI: 10.1109/tsp.2017.2712122

Cao, Y., Chang, G.B., Feng, Y. et al.: 2024, Statistically optimal Slepian method for processing gravity level 2 data. Acta Geodyn. Geomater., 21, 37–50. DOI: 10.13168/agg.2024.0004

Chambers, D.P., Wahr, J. and Nerem, R.S.: 2004, Preliminary observations of global ocean mass variations with GRACE. Geophys. Res. Lett., 31, 4. DOI: 10.1029/2004gl020461

Chen, J., Tapley, B., Tamisiea, M.E. et al.: 2021, Error assessment of GRACE and GRACE Follow-On Mass Change. J. Geophys. Res., Solid Earth, 126. DOI: 10.1029/2021JB022124

Chen, Q.J., Shen, Y.Z., Chen, W. et al.: 2016, An improved GRACE monthly gravity field solution by modeling the non-conservative acceleration and attitude observation errors. J. Geod., 90, 503–523. DOI: 10.1007/s00190-016-0889-6

Cheng, S., Yuan, L.G., Jiang, Z.S. et al.: 2021, Investigating terrestrial water storage change in Sichuan, Yunnan and Chongqing using Slepian basis functions. Chinese J. Geophys-CH, 64, 1167–1180. DOI. 10.6038/cjg202100194

Crowley, J.W. and Huang, J.L.: 2020, A least-squares method for estimating the correlated error of GRACE models. Geophys. J. Int., 221, 1736–1749. DOI: 10.1093/gji/ggaa104

Feng, Y., Yu, Y., Zhang, S. et al.: 2024, Suppressing stripe noise in GRACE/GFO level-2 products with dual low-pass filtering. Acta Geod. Geophys., 59, 405–425. DOI: 10.1007/s40328-024-00448-9

Galindo, F.J. and Palacio, J.: 2003, Post-processing ROA data clocks for optimal stability in the ensemble timescale. Metrologia, 40, S237–S244. DOI: 10.1088/0026-1394/40/3/301

Golub, G.H., Heath, M. and Wahba, G.: 1979, Generalized cross-validation as a method for choosing a good ridge parameter. Technometrics, 21, 215–223. DOI: 10.1080/00401706.1979.10489751

Hansen, P.C and O'Leary, D.P.: 1993, The use of the L-curve in the regularization of discrete Ill-posed problems. SIAM J. Sci. Comput., 14, 1487–1503. DOI: 10.1137/0914086

Harig, C. and Simons, F.J.: 2012, Mapping Greenland's mass loss in space and time. Proc. Natl. Acad. Sci. USA, 109, 19934–19937. DOI: 10.1073/pnas.1206785109

Hoerl, A.E. and Kennard, R.W.: 2000, Ridge regression: Biased estimation for nonorthogonal problems. Technometrics, 12, 55–67. DOI: 10.1080/00401706.1970.10488634

Ji, K.P., Shen, Y.Z., Chen, Q.J. et al.: 2022, An adaptive regularized solution to Inverse Ill-Posed Models. IEEE Trans. Geosci. Remote Sens., 60, 15. DOI: 10.1109/tgrs.2022.3205572

Koot, L., Viron, O.d. and Dehant, V.: 2006, Atmospheric angular momentum time-series: Characterization of their internal noise and creation of a combined series. J. Geod., 79, 663–674. DOI: 10.1007/s00190-005-0019-3

Kusche, J.: 2007, Approximate decorrelation and non-isotropic smoothing of time-variable GRACE-type gravity field models. J. Geod., 81, 733–749. DOI: 10.1007/s00190-007-0143-3

Kusche, J., Schmidt, R., Petrovic, S. et al.: 2009, Decorrelated GRACE time-variable gravity solutions by GFZ, and their validation using a hydrological model. J. Geod., 83, 903–913. DOI: 10.1007/s00190-009-0308-3

Luthcke, S.B., Rowlands, D.D., Lemoine, F.G. et al.: 2006, Monthly spherical harmonic gravity field solutions determined from GRACE inter-satellite range-rate data alone. Geophys. Res. Let., 33, 4. DOI: 10.1029/2005gl024846

Plattner, A. and Simons, F.J.: 2015, High-resolution local magnetic field models for the Martian South Pole from Mars Global Surveyor data. J. Geophys. Res. Planets, 120, 1543–1566. DOI: 10.1002/2015je004869

Qian, N.J., Chang, G.B., Ditmar, P. et al.: 2022, Sparse DDK: A data-driven decorrelation filter for GRACE Level-2 products. Remote Sens., 14, 24. DOI: 10.3390/rs14122810

Qian, N.J., Chang, G.B., Gao, J.X. et al.: 2021, Vehicle's instantaneous velocity reconstruction by combining GNSS Doppler and Carrier Phase measurements through Tikhonov regularized Kernel learning. IEEE Trans. Veh. Technol., 70, 4190–4202. DOI: 10.1109/tvt.2021.3076056

Sasgen, I., Martinec, Z. and Fleming, K.: 2006, Wiener optimal filtering of GRACE data. Stud. Geophys. Geod., 50, 499–508. DOI: 10.1007/s11200-006-0031-y

Shen, Y., Xu, P. and Li, B.: 2012, Bias-corrected regularized solution to inverse ill-posed models. J. Geod., 86, 597–608. DOI: 10.1007/s00190-012-0542-y

Simons, F.J. and Dahlen, F.A.: 2006, Spherical Slepian functions and the polar gap in geodesy. Geophys. J. Int., 166, 1039–1061. DOI: 10.1111/j.1365-246X.2006.03065.x

Tapley, B.D., Bettadpur, S., Ries, J.C. et al.: 2004, GRACE measurements of mass variability in the Earth system. Science, 305, 503-505. DOI: 10.1126/science.1099192

Velicogna, I. and Wahr, J.: 2006, Acceleration of Greenland ice mass loss in spring 2004. Nature, 443, 329–331. DOI: 10.1038/nature05168

Wahr, J., Molenaar, M. and Bryan, F.: 1998, Time variability of the Earth's gravity field: Hydrological and oceanic effects and their possible detection using GRACE. J. Geophys. Res., Solid Earth, 103, 30205–30229. DOI: 10.1029/98jb02844

Xu, P.: 1992, Determination of surface gravity anomalies using gradiometric observables. Geophys. J. Int., 110, 321–332. DOI: 10.1111/j.1365-246X.1992.tb00877.x

Yang, T.L., Yu, H.W. and Wang, Y.: 2022, An efficient low-pass-filtering algorithm to de-noise global GRACE data. Remote Sens. Environ., 283, 15. DOI: 10.1016/j.rse.2022.113303

**APPENDIX I TCH CALCULATION FORMULA**

Suppose there are N different observation sequences, denoted as $X_i$ (i=1,2,3,4,…*N)*. Among them, i represents the results obtained by different methods. Then each observation sequence can be expressed by the following formula:

$$X_i = X_{\text{true}} + \varepsilon_i, \quad \forall i = 1,2,\cdots,N, \tag{24}$$

Among them, $X_{true}$ is the true signal, and εi is the error of the i-th method. However, since the true value cannot be obtained, we select any observation sequence as the reference value and calculate the difference sequence between the remaining observation sequences and this reference value. (Koot et al., 2006)

$$y_i = X_i - X_R = \varepsilon_i - \varepsilon_R, i = 1,2,\cdots,N-1 \tag{25}$$

CSR mascon data is used as a reference, then store the N-1 difference sequences in matrix Y.

$$\mathbf{Y} = \begin{bmatrix} y_{11} & y_{12} & \cdots & y_{1(N-1)} \\ y_{21} & y_{22} & \cdots & y_{2(N-1)} \\ \vdots & \vdots & \ddots & \vdots \\ y_{M1} & y_{M2} & \cdots & y_{M(N-1)} \end{bmatrix} \tag{26}$$

**M** is the number of observed values. Then the covariance matrix of the differences is as follows:

$$\mathbf{S} = \text{cov}(\mathbf{Y}) = \begin{bmatrix} s_{11} & s_{12} & \cdots & s_{1(N-1)} \\ s_{21} & s_{22} & \cdots & s_{2(N-1)} \\ \vdots & \vdots & \ddots & \vdots \\ s_{(N-1)1} & s_{(N-1)2} & \cdots & s_{(N-1)(N-1)} \end{bmatrix} \tag{27}$$

Introduce an unknown N*N noise covariance matrix **R**. Note that here **R** is a symmetric matrix, and its relationship with **S** is as follows (Galindo and Palacio, 2003):

$$S = J \cdot R \cdot J^T \tag{28}$$

In the formula, the matrices **J** and **R** are respectively translated as follows:

$$\mathbf{J}_{N-1,N} = \begin{bmatrix} 1 & 0 & \cdots & 0 & -1 \\ 0 & 1 & \cdots & 0 & -1 \\ \vdots & \vdots & \ddots & \vdots & \vdots \\ 0 & 0 & 0 & \cdots & -1 \end{bmatrix} \mathbf{R} = \begin{bmatrix} r_{11} & r_{12} & \cdots & r_{1N} \\ r_{12} & r_{22} & \cdots & r_{2N} \\ \vdots & \vdots & \ddots & \vdots \\ r_{1N} & r_{2N} & \cdots & r_{NN} \end{bmatrix} \tag{29}$$

Then it can be obtained that, since we need to solve for N*(N + 1)/2 unknown parameters, which is the number of different elements in **R**, but there are only N*(N - 1)/2 equations, which is the number of different elements in **S**. Obviously, **R** cannot be solved in this way. Therefore, the remaining N free parameters need to be obtained in a reasonable way to get a unique solution. According to the constraints proposed by Tavella and Premoli (1994) and improved by Galindo and Palacio (1999), a constraint function more suitable for the Kuhn - Tucker theory is given.

$$H_2(r_{1N,\ldots},r_{NN}) = -\frac{H_1(r_{1N,\ldots,}r_{NN})}{K} < 0, \tag{30}$$

where $K = \sqrt[N-1]{|S|}$,,$H_1(r_{1N},\ldots,r_{NN})$ is the constraint condition proposed by Tavella and Premoli (1994).

$$H_1(r_{1N,\ldots,}r_{NN}) = \frac{|R|}{|S|} = r_{NN} - [r_{1N} - r_{NN},\cdots,r_{(N-1)N} - r_{NN}]S^{-1}[r_{1N} - r_{NN},\cdots,r_{(N-1)N} - r_{NN}]^T \tag{31}$$

$$F_1(r_{1N},\cdots,r_{NN}) = \frac{1}{K^2} \cdot \sum_{i<j}^{N} r_{ij}^2 \tag{32}$$

In order to make the initial value within the constraint conditions, set the initial value of the iterative calculation as follows:

$$r_{iN}^0 = 0 \quad i < N$$
$$r_{NN}^0 = \frac{1}{2s^*}, s^* = [1,\cdots,1]S^{-1}[1,\cdots,1]^T \tag{33}$$

Then, according to the constraints, the N free parameters can be obtained by minimizing the objective function.